Numerical simulation of tsunami wave heights and currents at the Institute of Ocean Sciences and Pacific Biological Station from a magnitude 9.2 1964-type Alaska earthquake

Isaac V. Fine and Richard E. Thomson

Fisheries and Oceans Canada
Institute of Ocean Sciences
9860 West Saanich Road
Sidney, BC V8L 4B2

2026

Canadian Technical Report of
Hydrography and Ocean Sciences 413

Fisheries and Oceans Canada | Pêches et Océans Canada

Canada

Canadian Technical Report of Hydrography and Ocean Sciences

Technical reports contain scientific and technical information of a type that represents a contribution to existing knowledge, but which is not normally found in the primary literature. The subject matter is generally related to programs and interests of the Oceans and Science sectors of Fisheries and Oceans Canada.

Technical reports may be cited as full publications. The correct citation appears above the abstract of each report. Each report is abstracted in the data base Aquatic Sciences and Fisheries Abstracts.

Technical reports are produced regionally but are numbered nationally. Requests for individual reports will be filled by the issuing establishment listed on the front cover and title page.

Regional and headquarters establishments of Ocean Science and Surveys ceased publication of their various report series as of December 1981. A complete listing of these publications and the last number issued under each title are published in the Canadian Journal of Fisheries and Aquatic Sciences, Volume 38: Index to Publications 1981. The current series began with Report Number 1 in January 1982.

Rapport technique canadien sur l'hydrographie et les sciences océaniques

Les rapports techniques contiennent des renseignements scientifiques et techniques qui constituent une contribution aux connaissances actuelles mais que l'on ne trouve pas normalement dans les revues scientifiques. Le sujet est généralement rattaché aux programmes et intérêts des secteurs des Océans et des Sciences de Pêches et Océans Canada.

Les rapports techniques peuvent être cités comme des publications à part entière. Le titre exact figure au-dessus du résumé de chaque rapport. Les rapports techniques sont résumés dans la base de données Résumés des sciences aquatiques et halieutiques.

Les rapports techniques sont produits à l'échelon régional, mais numérotés à l'échelon national. Les demandes de rapports seront satisfaites par l'établissement auteur dont le nom figure sur la couverture et la page de titre.

Les établissements de l’ancien secteur des Sciences et Levés océaniques dans les régions et à l'administration centrale ont cessé de publier leurs diverses séries de rapports en décembre 1981. Vous trouverez dans l'index des publications du volume 38 du Journal canadien des sciences halieutiques et aquatiques, la liste de ces publications ainsi que le dernier numéro paru dans chaque catégorie. La nouvelle série a commencé avec la publication du rapport numéro 1 en janvier 1982.

Canadian Technical Report of
Hydrography and Ocean Sciences 413

2026

NUMERICAL SIMULATION OF TSUNAMI WAVE HEIGHTS AND CURRENTS AT THE INSTITUTE OF OCEAN SCIENCES AND PACIFIC BIOLOGICAL STATION FROM A MAGNITUDE 9.2 1964-TYPE ALASKA EARTHQUAKE

by

Isaac V. Fine and Richard E. Thomson

Fisheries and Oceans Canada
Institute of Ocean Sciences
9860 West Saanich Road
Sidney, BC V8L 4B2

Cat. No. Fs 97-18/413E-PDF ISBN 978-0-660-99243-3 ISSN 1488-5417

Correct citation for this publication:

Fine, I.V., and Thomson, R.E. 2026. Numerical simulation of tsunami wave heights and currents at the Institute of Ocean Sciences and Pacific Biological Station from a magnitude 9.2 1964-type Alaska earthquake. Can. Tech. Rep. Hydrogr. Ocean Sci. 413: v + 27 p.

TABLE OF CONTENTS

1. INTRODUCTION: GREAT ALASKA 1964 EARTHQUAKE AND TSUNAMI 1

2. SETUP OF THE NUMERICAL MODEL 3

2.1. NESTED GRID FORMULATION 3

2.2. TSUNAMI SOURCE 4

3. RESULTS FOR COARSE AND MEDIUM GRIDS 4

3.1. COMPARISON WITH THE OBSERVED RECORD FROM THE FULFORD HARBOUR TIDE GAUGE 4

3.2. MAXIMUM TSUNAMI WAVE HEIGHTS 7

4. RESULTS FOR PATRICIA BAY: WAVE HEIGHTS AND TSUNAMI-INDUCED CURRENTS 9

5. RESULTS FOR THE PACIFIC BIOLOGICAL STATION: TSUNAMI WAVE HEIGHTS AND TSUNAMI-INDUCED CURRENTS 17

6. CONCLUSIONS 25

ACKNOWLEDGEMENTS 26

REFERENCES 26

ABSTRACT

Fine, I.V., and Thomson, R.E. 2026. Numerical simulation of tsunami wave heights and currents at the Institute of Ocean Sciences and Pacific Biological Station from a magnitude 9.2 1964-type Alaska earthquake. Can. Tech. Rep. Hydrogr. Ocean Sci. 413: v + 27 p.

The magnitude 9.2 Kodiak Alaska earthquake of March 28, 1964 was the second strongest earthquake recorded in the World Ocean. This study uses a state-of-the-art numerical model to simulate a future tsunamigenic event of magnitude 9.2 off Alaska to determine the wave heights and currents that will impact the marine facilities at the Institute of Ocean Sciences in Patricia Bay (Sidney) and the Pacific Biological Station in Departure Bay (Nanaimo). The model is based on newly available high-resolution bathymetric and topographic data and is validated using tsunami wave measurements recorded at Fulford Harbour in the Canadian Gulf Islands following the 1964 earthquake. The main findings of the modeling are: (1) The tsunami at the Institute of Ocean Sciences will reach 0.36 m above the tidal level at the time of the wave arrivals and the third wave will be the highest; (2) the tsunami at the Pacific Biological Station will reach 0.16 m above the tidal level at the time of the wave arrivals and the first wave will be the highest; and (3) maximum tsunami-induced current speeds will be below 0.2 m/s (0.4 knots) at both sites. We conclude that a future 1964-type event under present-day sea level conditions is unlikely to cause significant flooding at the two sites. However, the tsunami hazard increases markedly under predicted global sea level rise conditions of over 1 metre by year 2100.

RÉSUMÉ

Fine, I.V., and Thomson, R.E. 2026. Numerical simulation of tsunami wave heights and currents at the Institute of Ocean Sciences and Pacific Biological Station from a magnitude 9.2 1964-type Alaska earthquake. Can. Tech. Rep. Hydrogr. Ocean Sci. 413: v + 27 p.

L'estimation du risque d'onde de tempête sur la côte de la Colombie-Britannique revêt une importance considérable pour les vastes zones basses de la province, comme la baie Boundary, dans le sud du détroit de Georgia. Un modèle océanique de Princeton bidimensionnel à grille imbriquée, intégrant une approche d'humidification-assèchement basée sur de nouvelles données bathymétriques et topographiques à haute résolution, a été utilisé pour simuler la hauteur des ondes de tempête dans la baie Boundary lors de six tempêtes historiques survenues dans la région du Grand Vancouver depuis 1981 : le 14 novembre 1981 ; le 16 décembre 1982 ; le 27 janvier 1983 ; le 1er janvier 1997 ; le 4 février 2006 ; et le 15 décembre 2006. Français Les principales conclusions sont les suivantes : (1) les hauteurs des ondes de tempête modélisées sont proches des valeurs observées aux marégraphes de Point Atkinson, Vancouver et Cherry Point (État de Washington), bien que dans certains cas le modèle sous-estime les hauteurs des ondes de 5 à 20 cm ; (2) après un léger ajustement, les amplitudes historiques estimées des ondes de tempête dans la baie Boundary varient de 0,91 m à 1,05 m au-dessus du niveau de la marée pour tous les événements ; et (3) la distribution des amplitudes des ondes de tempête dans la baie Boundary n'est pas uniforme, les amplitudes les plus élevées affectant l'extrémité nord-est de la région (baie Mud). Dans la région de Semiahmoo, les amplitudes sont jusqu'à 5 cm inférieures à celles de la baie Mud. Les hauteurs des ondes de tempête dans cette étude sont déterminées pour la marée moyenne des hautes eaux plus hautes ; pour déterminer l'étendue des inondations côtières lors d'événements similaires à l'avenir, les marées prévues au moment de la tempête doivent être prises en compte.

Port Alberni, March 1964. Photo from http://lesleefarrell.com/properties/extraordinary-shoal-point-penthouse.

1. INTRODUCTION: GREAT ALASKA 1964 EARTHQUAKE AND TSUNAMI

The second strongest instrumentally recorded earthquake in the World Ocean (M_w 9.2) occurred off Alaska on March 28, 1964. The event generated a catastrophic tsunami, the second greatest in the 20th century after the 1960 Chilean tsunami, with maximum wave heights of 20 m near the earthquake source region. A large number of landslides and submarine landslides were also initiated, resulting in local tsunami waves as high as 70 m (Lander, 1996). The earthquake, which was the strongest instrumentally recorded earthquake in the North Pacific and second in magnitude only to the M_w 9.5 Chilean earthquake in 1960, occurred in the vicinity of Prince William Sound, leading to widely used name of the "Prince William Sound Earthquake" (Spaeth and Berkman, 1967). Because of the event date (28 March 1964), the earthquake and associated Pacific-wide tsunami are also called the "Good Friday Earthquake and Tsunami".

The Good Friday tsunami was responsible for close to 130 deaths and about million dollars in damage in Alaska, Washington, California and Hawaii (Spaeth and Berkman, 1967; Lander, 1996). Several locations on the coast of British Columbia experienced major damage (Clague et al., 2003; Anderson and Gow, 2004), with the highest wave ever

recorded in Canada occurring at Shields Bay on the west coast of Graham Island (Haida Gwaii). Here, a wave crest was reported to be 5.2 m above the spring high water, or 9.8 m above tidal datum. Most of the damage from the tsunami occurred in Port Alberni, where a wave reached 4.2 m above the spring-tide high water (Dunbar et al., 1991; Fine et al., 2008).

Several numerical models have been constructed to simulate tsunami wave propagation from the 1964 event in the northeast Pacific Ocean (cf. Dunbar et al., 1991; Myers and Baptista, 2001). Although these studies were able to simulate the main features of the tsunami impact on the British Columbia Coast, a more detailed analysis based on recent high-resolution bathymetry and a more refined high-resolution source region of the uplift distribution is needed. Because of its exceptional characteristics, the 1964 Alaska tsunami is typically considered as a proxy for a major future tsunami along the Pacific coast of North America (Suleimani et al., 2013).

The purpose of this report is to simulate the expected tsunami waves for the Institute of Ocean Sciences (and co-located Canadian Coast Guard Station) at Patricia Bay, Sidney, and at the Pacific Biological Station in Departure Bay, Nanaimo, that would be generated by an Alaska 1964-type earthquake having a moment magnitude $Mw \sim 9.2$. This work is part of a larger study to inform future upgrades and redesigns of Coast Guard stations around the British Columbia coast in order to mitigate the impact of hazardous long-wave events on the operability of these stations (see also Fine et al., 2018a,b).

2. SETUP OF THE NUMERICAL MODEL

2.1. NESTED GRID FORMULATION

The basics of nested grid formulation for numerical tsunami models is described in Fine et al. (2018a,b). Accurate numerical simulation of tsunami waves in the rapidly shoaling regions of the west coast of British Columbia requires setting up the model domain as a series of nested grids of ever finer spatial and temporal resolution. The use of nested grids of smaller cell dimensions and time steps makes it possible to resolve tsunami wave configurations as they propagate into shallow coastal regions. The principal requirements for numerical models using nested grids are as follows:

Nested grid cell sizes are generally obtained by dividing the initial, large-scale coarse numerical grid by an integer, typically 3 to 5. Integers larger than this can lead to grid interface problems:

- Nested grids are needed in near-coastal areas; the coarse "parent" grid should be of sufficient extent to resolve possible feed-back effects that the nested grid may have on the parent grid during the simulation time;
- A good interface between the inner and outer domains is required to avoid errors and model instability associated with point matching between the different grids. This should allow two-way fluxes without trapping shorter waves at the inner domain boundaries;
- High resolution bathymetry, external forcing and observations are needed for model domain setup, initialization and validation at each domain level; here, the nested-grid formulation is similar to that used in well-known tsunami models, TUNAMI and COMCOT (Liu et al., 1998; Imamura et al., 2006; Wang, 2009).

Dispersion effects can be included in the model by substituting numerical dispersion for the actual physical dispersion. Solving this issue (see for example, Imamura et al., 1988) has made it possible for investigators to cover large, open ocean regions, representative of an area affected by a 1964 style tsunami, using a relatively coarse grid with a cell size of roughly 10 km by 10 km (4-5 arc-minutes).

This study uses a series of four nested grids for the Alaska 1964 tsunami model (Table 1). In general, our choice of model grids allows us to account for the need for high spatial resolution to accurately resolve the reflection and transformation of the waves and for the need for large spatial extent to capture the effects of frequency dispersion during long distance wave propagation. However, because of the relatively long periods of the tsunamis generated in the deep-water source regions used in this study, and because of the relatively short propagation times of 4-5 hours between the source region and Patricia Bay and Departure Bay, the dispersion effect is negligible. In this case, high bathymetric resolution is the important factor for modelling wave propagation in the offshore regions.

2.2. TSUNAMI SOURCE

Numerical simulation of the 1964 tsunami is based on the revised (Suleimani et al., 2013) coseismic slip distribution for the 1964 rupture based on the model of Suito and Freymueller (2009). The description of the model is published in Fine et al. (2018a,b). The tsunami simulations in the Fine et al. studies reveal that, including deformation due to horizontal displacements in the source function, result in an increase in the far-field tsunami amplitudes. The resulting vertical coseismic deformation is shown in Figure 1.

3. RESULTS FOR COARSE AND MEDIUM GRIDS

3.1. COMPARISON WITH THE OBSERVED RECORD FROM THE FULFORD HARBOUR TIDE GAUGE

To verify the numerical model, we compared the modelled waves for the 1964 Alaska tsunami with those recorded by the Fulford Harbour tide gauge (for the location, see Figure 5 below). The original analogue record of the tsunami was first digitized and the tides then carefully subtracted from the digital record using tidal analysis programs (cf. Thomson and Emery, 2024). The observed record is published in Rabinovich et al. (2019).

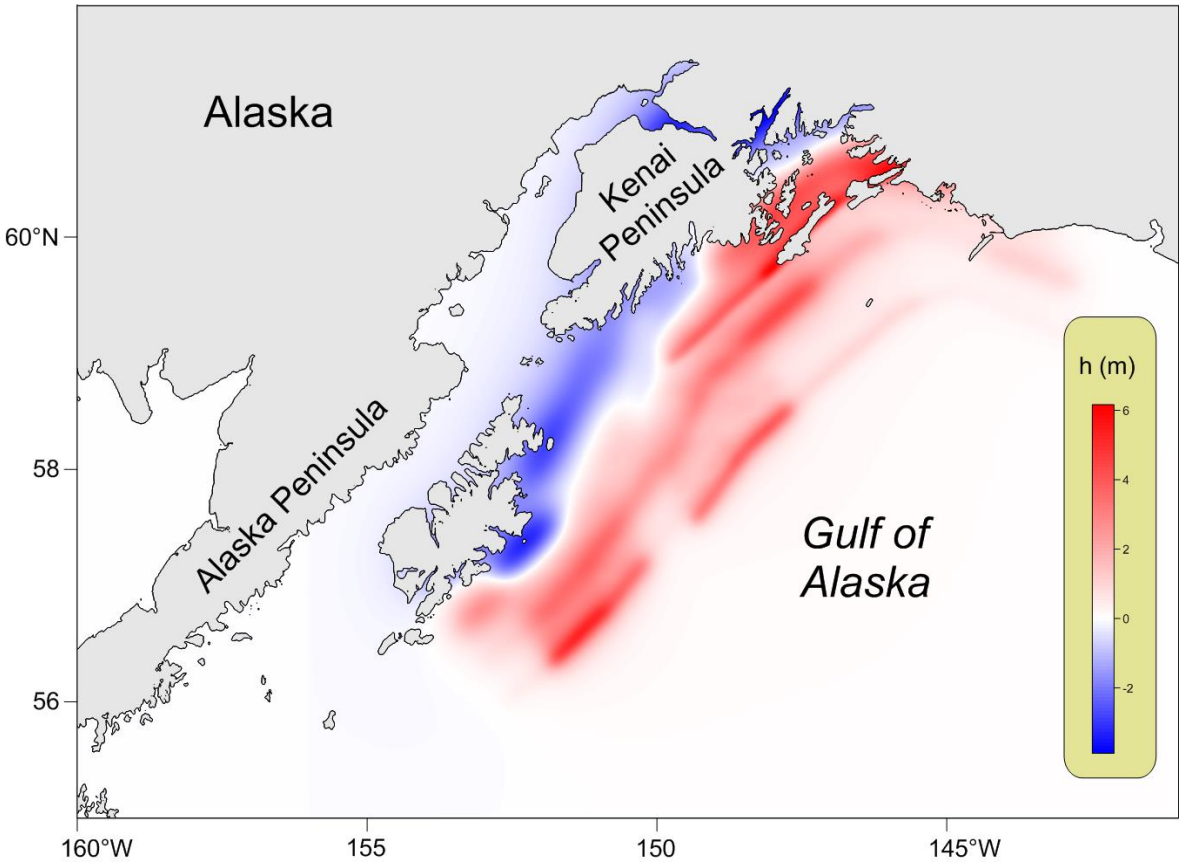

Figure 1. Vertical seafloor displacements (*h*, m) at the earthquake source region for the March 1964 Alaska tsunami (from Suleimani et al., 2013; Fine et al., 2018a,b). Seafloor displacements range from roughly -3 m (blue) to +6 m (red).

Comparisons of the observed and modelled waves are shown in Figure 2 and Table 3. It is evident that the modelled record closely fits the observed record . For both the observed and simulated records, the first wave is a crest wave and is the highest wave in the records. The travel times for the highest waves coincide within 5 minutes, indicating that the wave forms are very similar, despite the fact that the observations were based on a digitized analogue record.

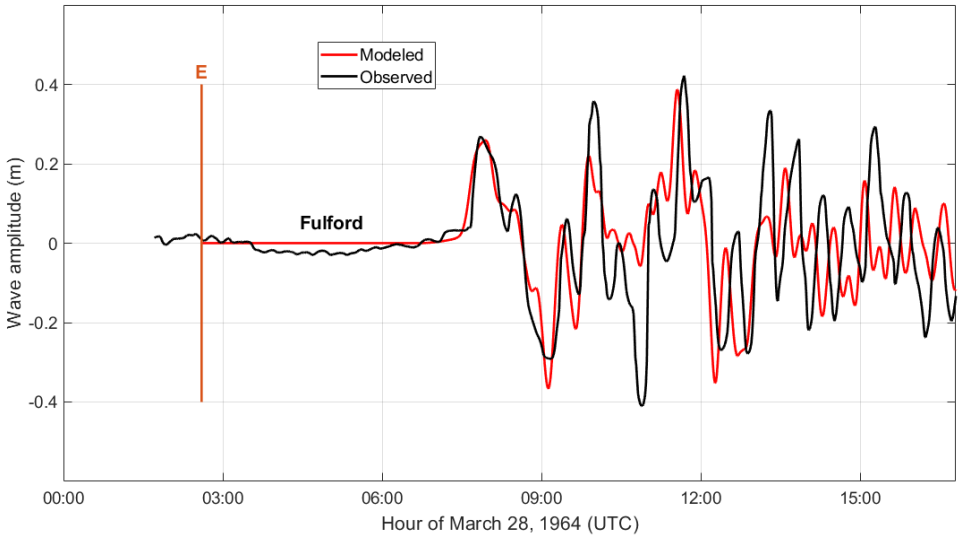

Figure 2. Observed versus modelled wave records for the March 1964 Alaska tsunami for the Fulford Harbour tide gauge site located in the Gulf Islands near Sidney, British Columbia (see Figure 5 for location). The letter "E" denotes the time of the earthquake.

Table 3. Statistical properties of the modelled and observed tsunami waves at the Fulford tide gauge location for the March 1964 tsunami source region. Wave heights are in metres and travel times in hours (h):minutes (min). UTC denotes Universal Coordinated Time.

Type	First wave		Maximum wave		Visible wave period (min)
	Amplitude (m)	Time of maximum elevation (UTC)	Amplitude (m)	Time of maximum elevation (UTC)	
Modelled	0.26	07:56	0.39	11:33	30, 110
Observed	0.27	07:51	0.42	11:41	30, 115

The maximum wave crest in the modelled record is just slightly lower (by 3-7%) than the maximum of the observed record; the times of wave maxima are within 8 minutes, which is surprisingly close in this instance given that the observations are from an analogue recording. Both records have similar waveforms, and the amplitudes and periods of the ensuing waves are also similar. The first 5 hours of the modeled record are highly correlated with the observations, with a correlation coefficient of 0.77 and a model skill number of

0.56. The high correlation between the observed and modeled records, combined with the high skill number, means that the tsunami source and model closely reproduce the properties of the event.

3.2. MAXIMUM TSUNAMI WAVE HEIGHTS

The computed distributions of wave height maxima for a future Alaska-type tsunami based on grids 1-2 are presented in Figures 3-4. Figure 3 shows the "rays" of maximum tsunami wave heights for the entire northeast Pacific. While tsunami wave-height maxima are found in Prince Williams Sound (the source area), considerable tsunami energy is radiated to the southeast toward the coast of California. In British Columbia and along the US West Coast, the most affected coastal zones are those exposed to the open ocean, such as the west coast of Vancouver Island, especially at the heads of the inlets, and the west coast of Washington State. In more protected areas, such as Juan de Fuca Strait, the computed tsunami wave amplitudes are markedly smaller (Figure 4; Grid 2).

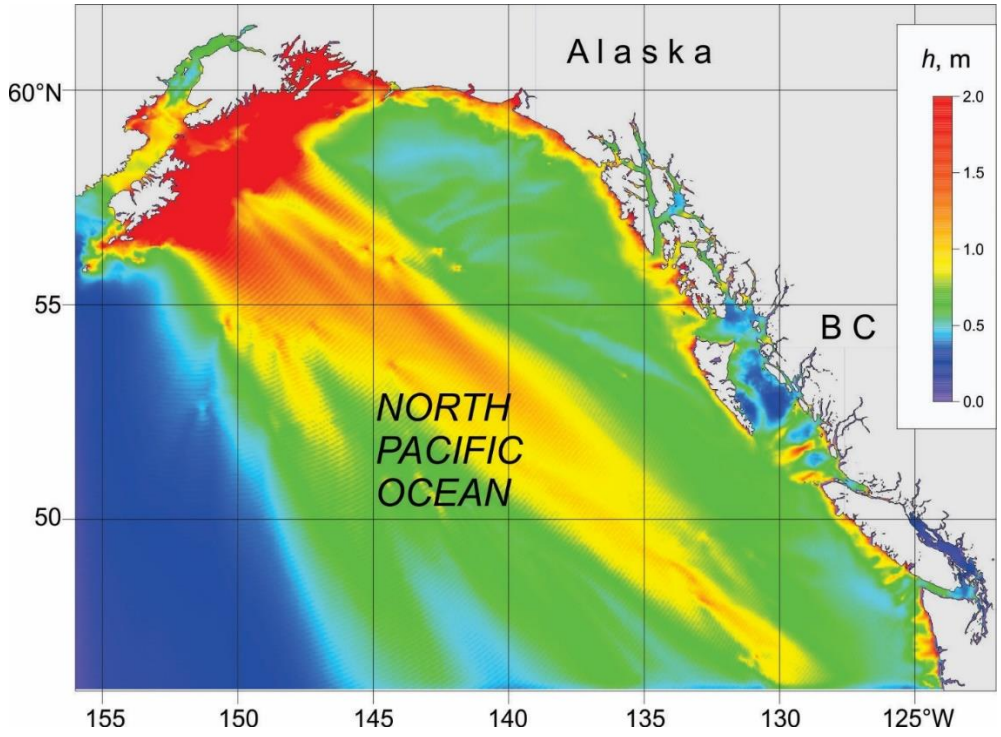

Figure 3. Distribution of maximum tsunami wave heights (*h*, metres) for Grid 1 of the nested-grid model for waves generated by simulation of the 1964 tsunami.

Results for the finer resolution grids (Grids 3-4) demonstrate the considerable spatial variability in the incoming tsunami wave heights for the study region. Figure 4

shows the distribution of the tsunami wave heights for Grid 3 in eastern Juan de Fuca Strait off Vancouver Island. As the figure indicates, wave amplitudes increase toward the shoreline and are especially high in the upper reaches of Victoria Harbour, where the wave amplitudes are 3-4 times higher than in the central part of Juan de Fuca Strait. The pronounced increase in tsunami wave heights in the harbours arises from resonance amplification of the incoming tsunami waves.

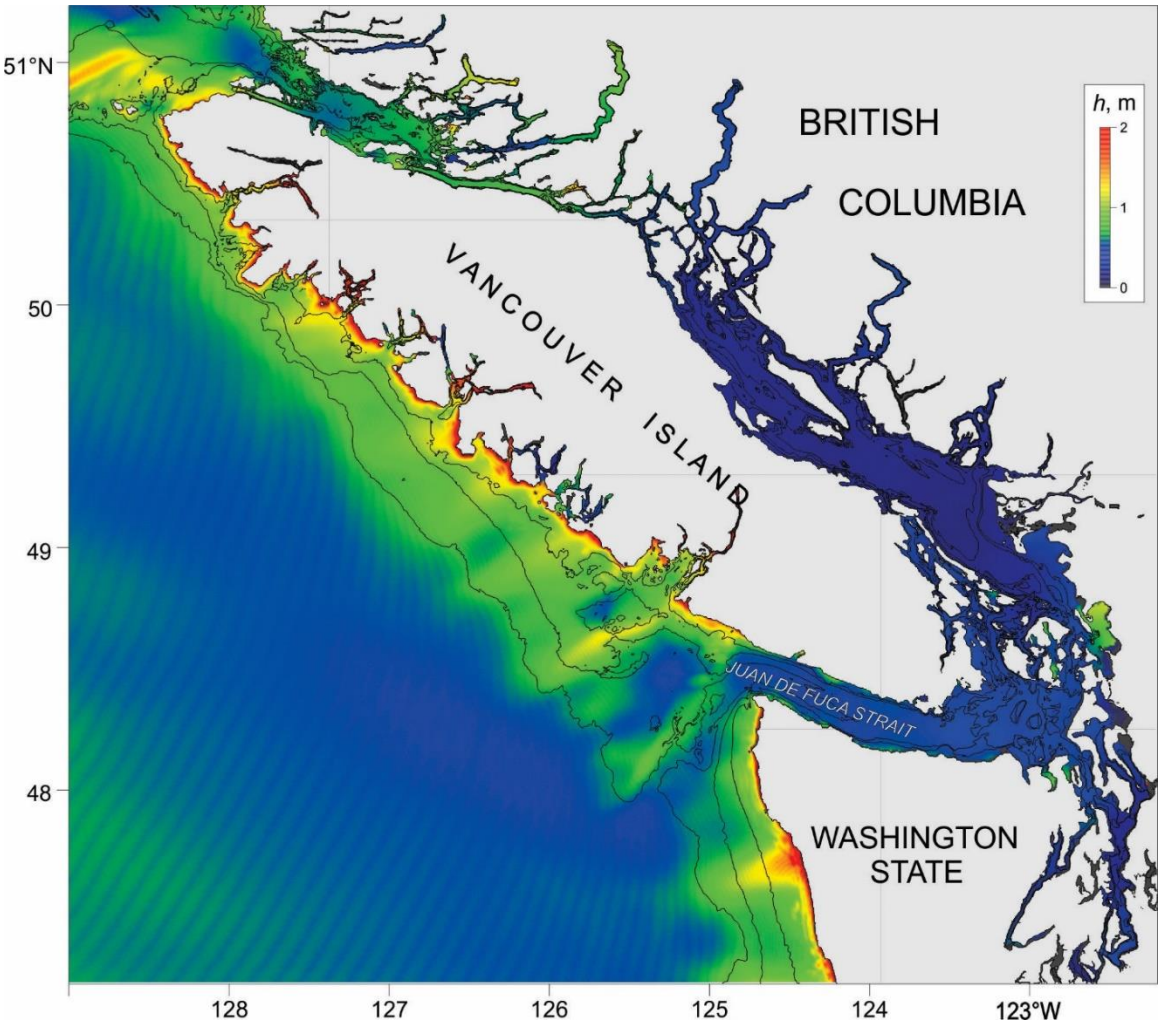

Figure 4. Distribution of maximum tsunami wave heights (*h*, metres) for Grid 2 of the nested-grid model for waves generated by simulation of the 1964 tsunami.

4. RESULTS FOR PATRICIA BAY: WAVE HEIGHTS AND TSUNAMI-INDUCED CURRENTS

Figure 5 presents a medium-high resolution map showing the distribution of the maximum tsunami heights in Saanich Inlet and vicinity. We note that the amplitudes of the tsunami waves gradually increase from the entrance toward the south (toward the head of the inlet) and toward the west, where they reach 0.5 m. In other parts of the inlet, the wave amplitudes are smaller, mostly less than 0.4 m. The general distribution is smooth for most of inlet, excluding some of the narrow channels.

A detailed map of the distribution of maximum tsunami amplitudes in Patricia Bay is shown in Figure 6. The tsunami waves in Patricia Bay undergo only small changes in amplitude, from 0.35 m to 0.39 m. The gradual change in tsunami amplitude within the bay is related to the frequencies of the waves, which, for this simulated event, are significantly lower than the fundamental frequency of the bay.

Figure 7 shows the simulated records of the tsunami heights at the sites A1-A12. Because of relatively low frequency (long periods) of the waves and the weak spatial gradient of their distribution, records at all sites are nearly identical. The travel time from the time of the earthquake is about 4 hours and 52 minutes for all records (we define arrival time as the time when the wave amplitude exceeds 1 cm). The first wave is a crest wave with a maximum amplitude of 0.35 m, which was achieved at 5 hours and 36 minutes after the earthquake. The third wave is the highest, with crest height of 0.37 m, which occurred at 9 hours and 11 minutes after the earthquake. The third wave also has the deepest trough of -0.45 m, which will occur 9 hours and 59 minutes after the quake. The tsunami waves have visible periods of about 2 hours.

Because of the low frequency of the tsunami waves, and the gradual spatial variations in the wave amplitudes over the bay, we would not expect strong tsunami-induced currents in the region. Indeed, maximum modeled currents in the bay (Figure 8) do not reach 0.2 m/s (0.4 knots). Because of focusing effects, current speeds marginally increase in areas having convex coastlines and decrease in areas that have concave coastlines.

Figures 9-14 show the simulated records of the eastward and northward components of tsunami-induced currents at sites A1-A12. The currents are clearly weak at all sites , which is to be expected given that current oscillations typically have periods of around 2 hours, i.e., roughly the same as that for sea-level oscillations. At the Coast Guard facility sites (Sites A6-A7), the current is less than 1 cm/s.

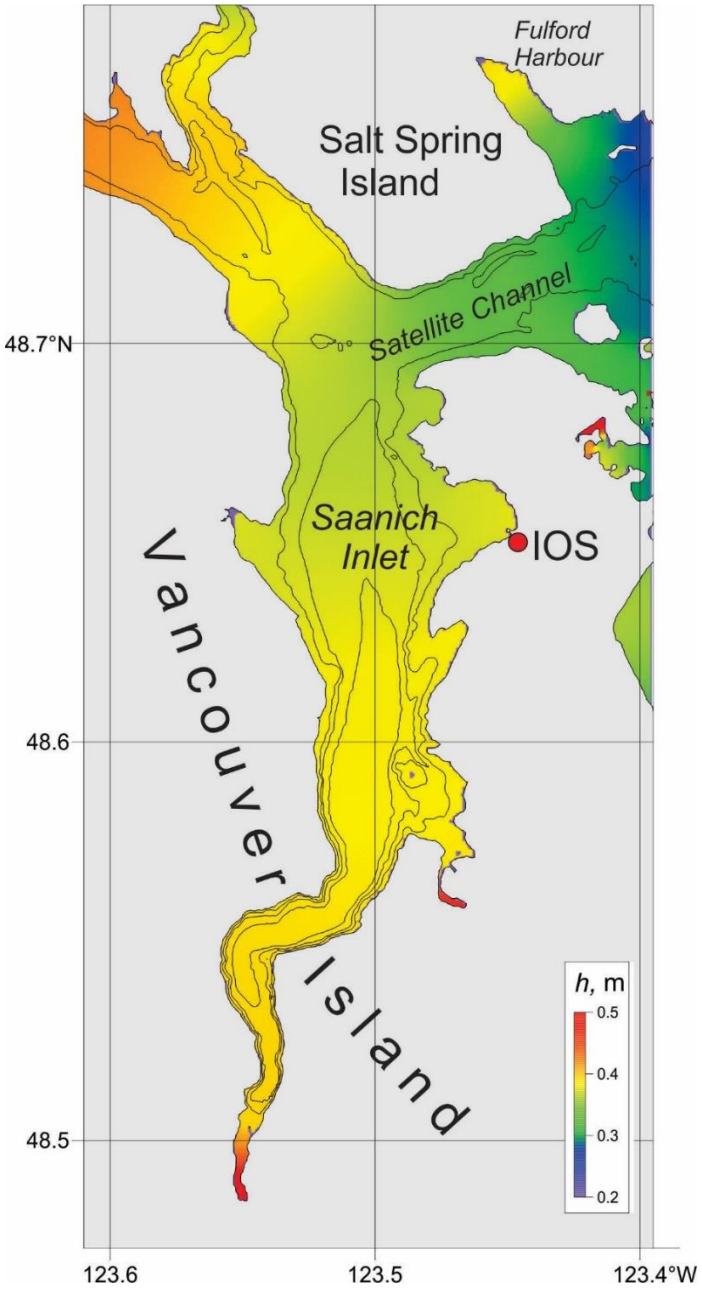

Figure 5. Distribution of maximum tsunami wave heights (*h*, metres) for Grid 3a (Saanich Inlet) of the nested-grid model for waves generated by simulation of a 1964-type Alaska tsunami. IOS shows the location of the Institute of Ocean Sciences.

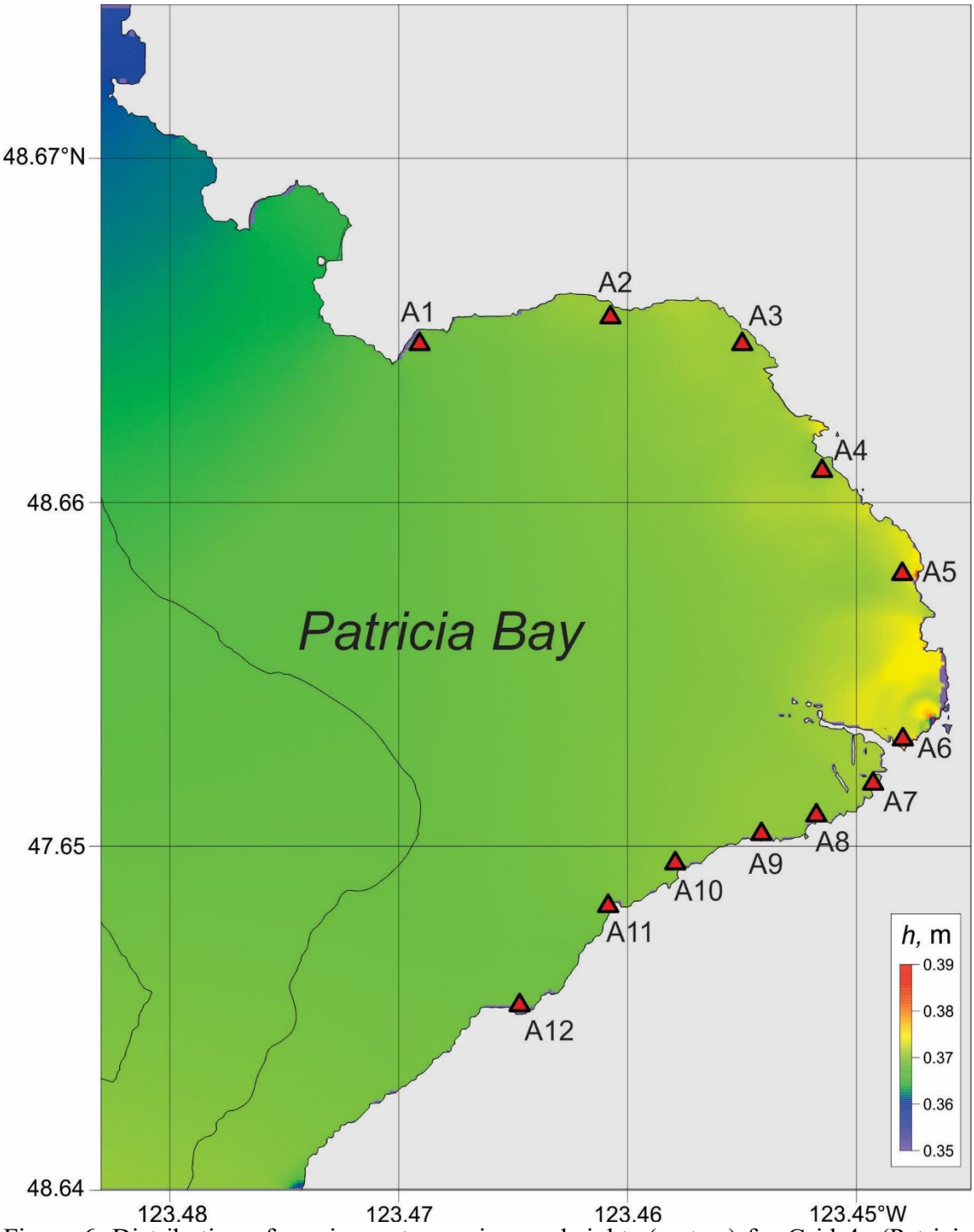

Figure 6. Distribution of maximum tsunami wave heights (metres) for Grid 4a (Patricia Bay, Saanich Inlet) of the nested-grid model for waves generated by simulation of a 1964-type Alaska tsunami.

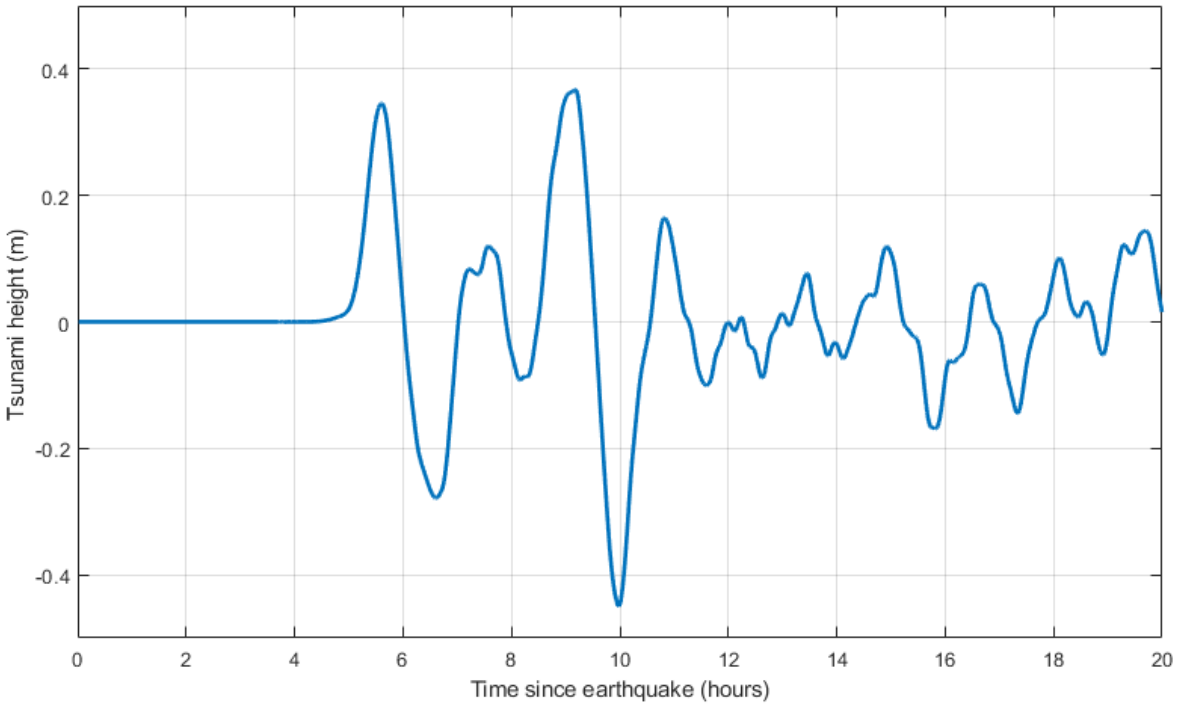

Figure 7. Simulated records of sea level variations arising from an Alaska 1964-type tsunami at Patricia Bay sites A1 – A12. See Figure 6 for the site locations. Note that the plots for all twelve time series (A1-A12) fall nearly on top of one another so that they

are not visible as separate curves in the figure.

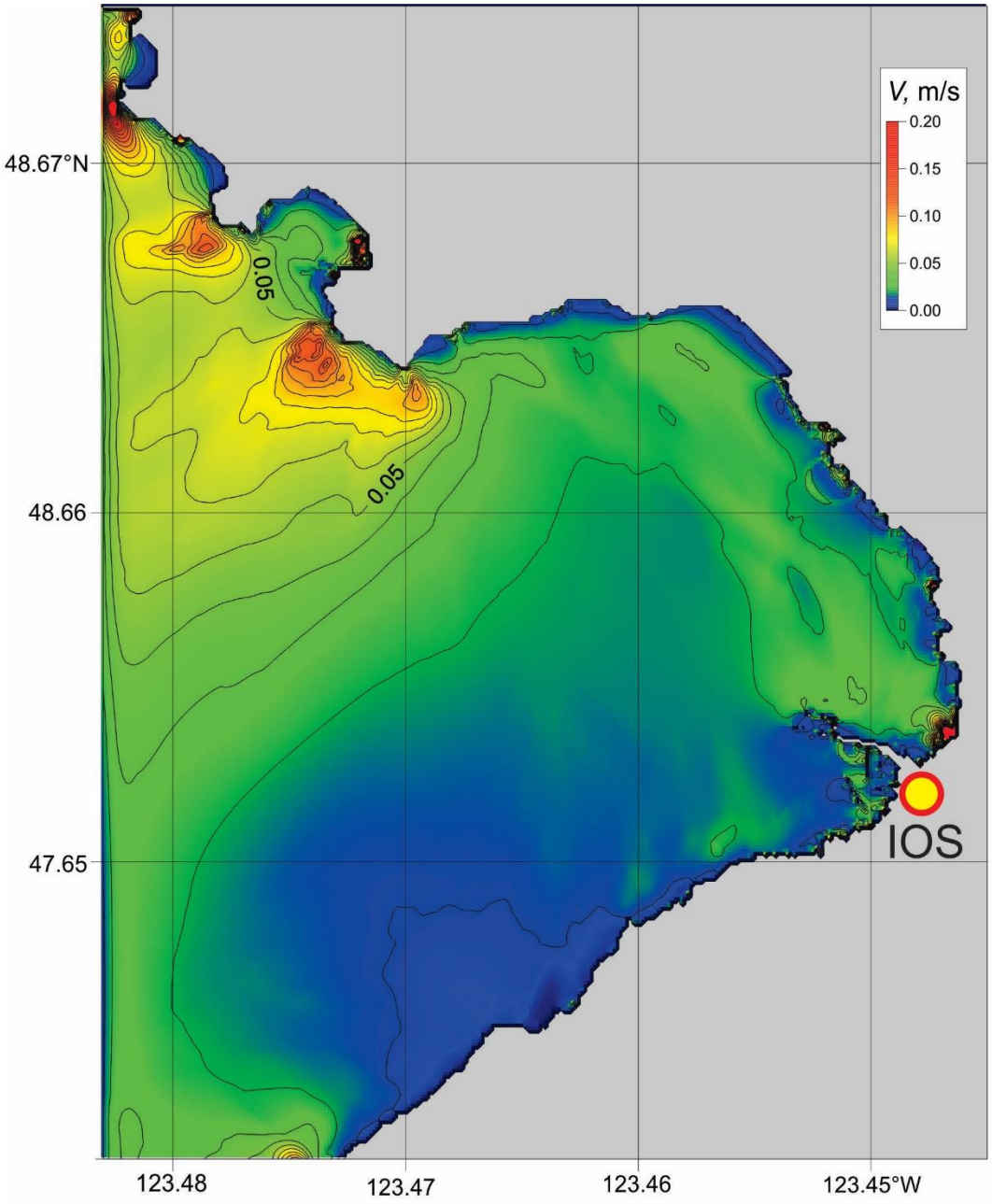

Figure 8. Distribution of the maximum tsunami-generated currents (V, m/s) for Grid 4a (Patricia Bay, Saanich Inlet) for simulation of a 1964-type Alaska tsunami. Strengthened currents occur near headlands. IOS = Institute of Ocean Sciences.

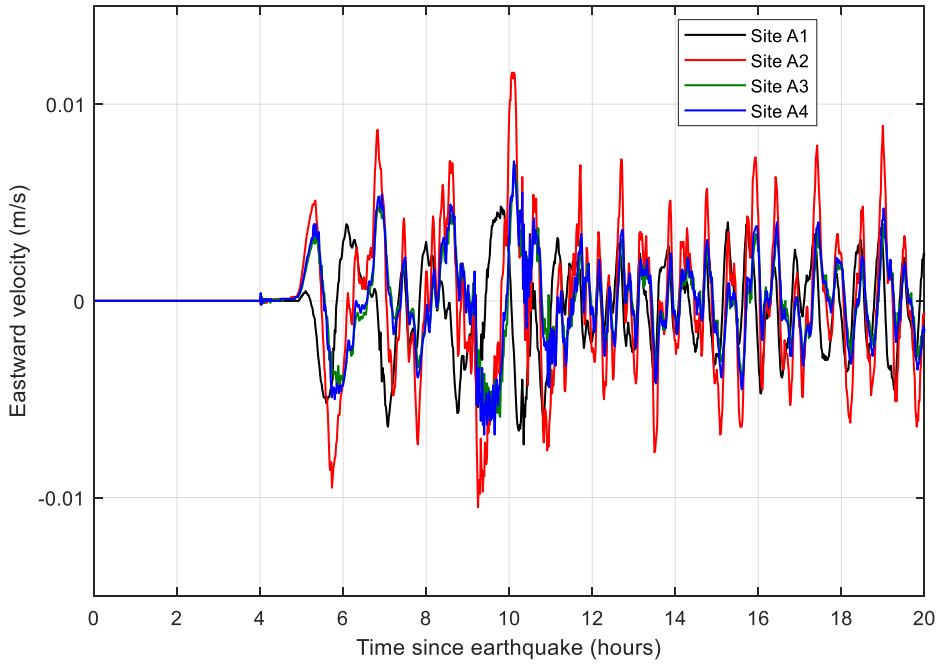

Figure 9. Simulated records of the eastward component of current velocity for an Alaska 1964-type tsunami at Patricia Bay sites A1, A2, A3 and A4 (See Figure 6 for the site locations).

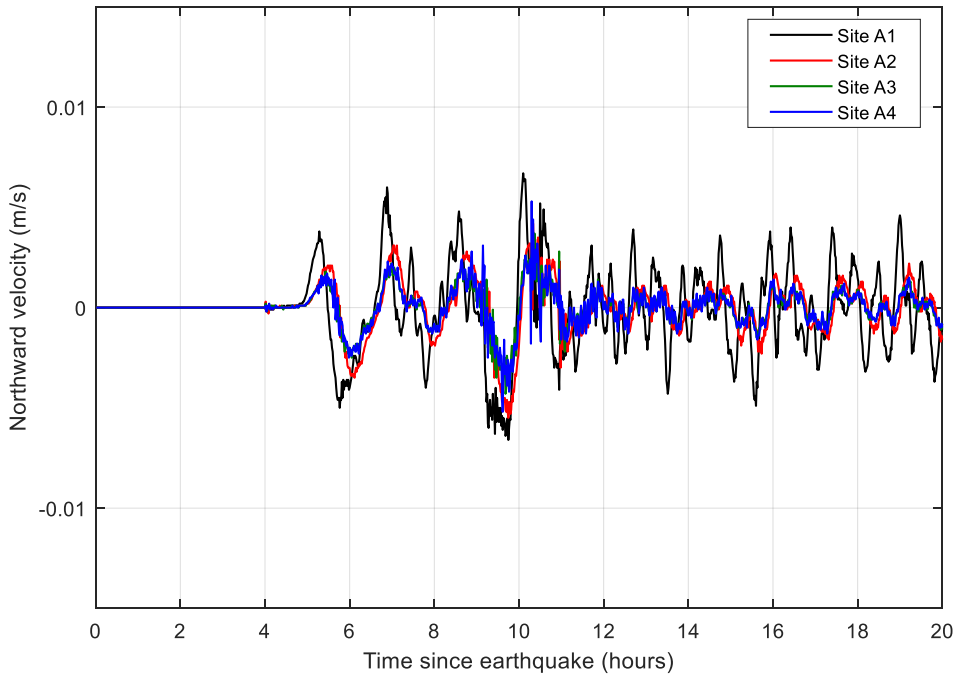

Figure 10. Simulated records of the northward component of current velocity for an Alaska 1964-type tsunami at Patricia Bay sites A1, A2, A3 and A4 (See Figure 6 for the site locations).

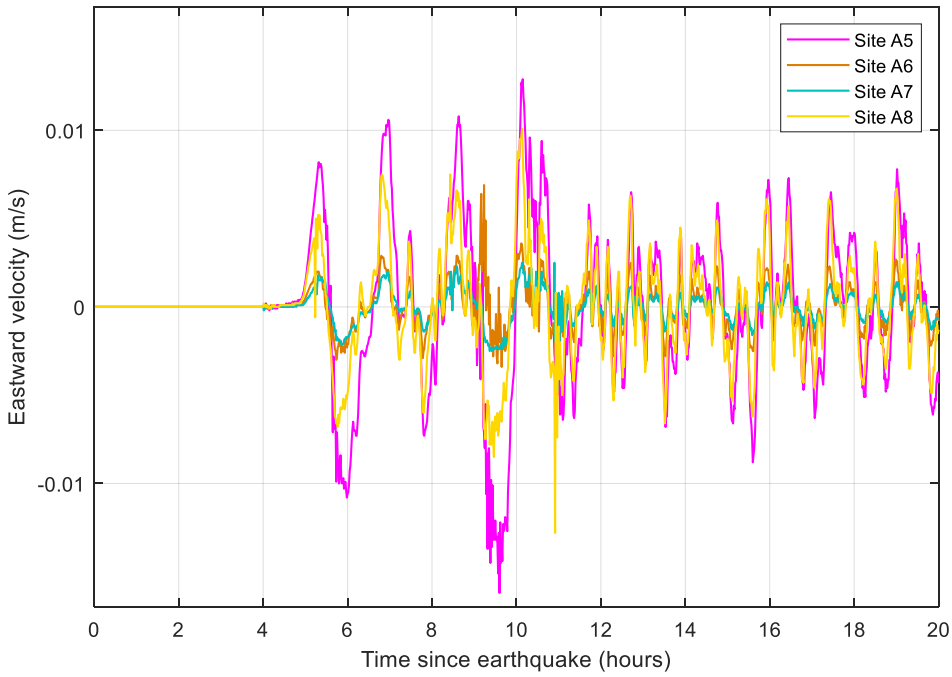

Figure 11. Simulated records of the eastward component of current velocity for an Alaska 1964-type tsunami at Patricia Bay sites A5, A6, A7 and A8 (See Figure 6 for the site locations).

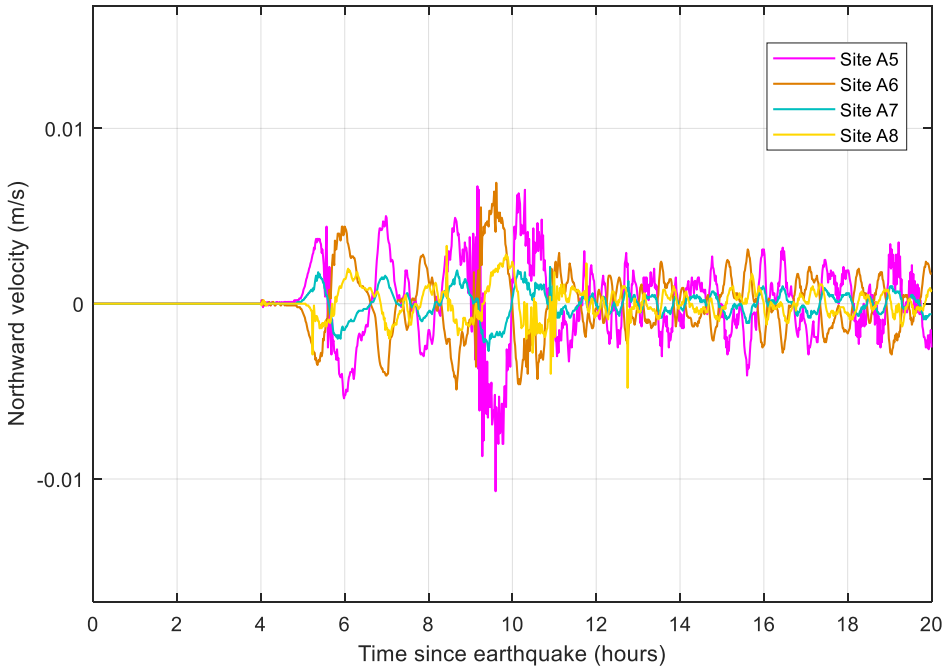

Figure 12. Simulated records of the northward component of current velocity for an Alaska 1964-type tsunami at sites A5, A6, A7 and A8 (See Figure 6 for the site locations).

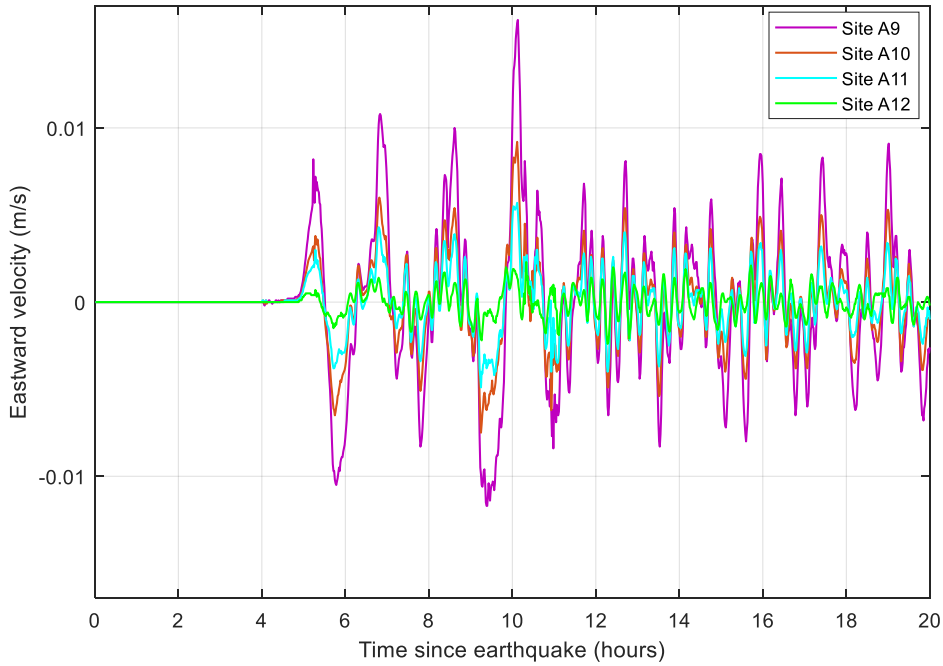

Figure 13. Simulated records of the eastward component of current velocity for the Alaska 1964-type tsunami at Patricia Bay sites A9, A10, A11 and A12 (See Figure 6 for the site locations).

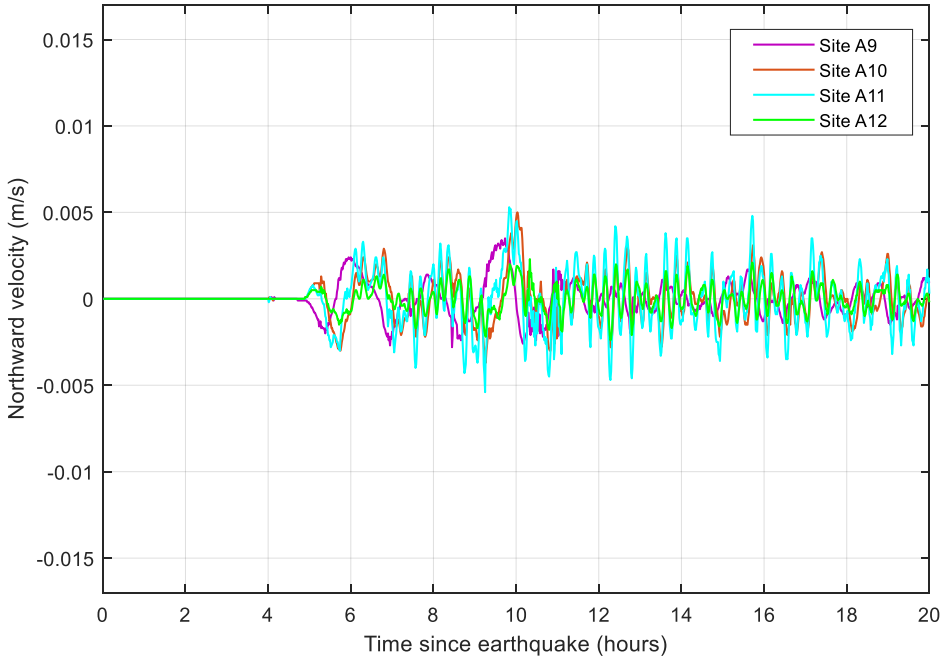

Figure 14. Simulated records of the northward component of current velocity for an Alaska 1964-type tsunami at Patricia Bay sites A9, A10, A11 and A12 (See Figure 6 for the site locations).

5. RESULTS FOR THE PACIFIC BIOLOGICAL STATION: TSUNAMI WAVE HEIGHTS AND TSUNAMI-INDUCED CURRENTS

Figure 15 presents a medium-high resolution map showing the distribution of maximum tsunami heights in the vicinity of Nanaimo for the 1964-type Alaska tsunami. The amplitudes of the waves are low, 0.16-0.18 m, over most of the region. In Stuart Channel, located to the south, and connected to the other areas by narrow passes, the tsunami waves are higher, but still less than 0.35 m.

The distribution of maximum tsunami amplitudes in Departure Bay is detailed in Figure 16. The modeled tsunami waves in the bay have small spatial variability, from 0.15 m to 0.17 m. Slightly higher waves are obtained for Newcastle Channel, separated from Newcastle Island by the main island. The gradual change in wave amplitudes over the bay are related to the frequency of the tsunami waves, which is significantly lower than the fundamental frequency of Departure Bay.

Figures 17-18 shows the simulated records of the tsunami heights at sites B1-B12. All records at the sites are remarkably close, with waves at sites B11 and B12 only marginally higher than at other sites. The travel time after the earthquake is about 5 hours and 33 minutes for all records (we define arrival time as the time when the wave amplitude first exceeds 1 cm). The first wave is a crest wave with a maximum amplitude that varies from 0.16 m (Site B7) to 0.17 m (Site B12), and is the highest wave in the records. The maximum wave height is reached 6 hours and 20 to 22 minutes after the earthquake. The deepest trough of -0.14 to -0.16 m occurs later, at 11 hours and 1 to 3 minutes after the earthquake. The tsunami waves have periods of about 2 hours.

As was the case for Patricia Bay, the low tsunami wave amplitudes, low frequency, and gradual spatial distribution of the tsunami amplitudes over the bay give rise to weak wave-induced currents. In this region, maximum currents in the bay (Figure 19) are less than 0.1 m/s (0.2 knots). The current increases at the entrance to Newcastle Channel, but only up to 0.2 m/s.

Figures 20-25 present the simulated records of the eastward and northward components of the tsunami-induced currents at the Departure Bay sites B1-B12. The currents at all sites are weak. Typical periods of the current oscillations are around 2 hours, or about the same as for the sea-level oscillations. At the Pacific Biological Station (Site B1) the current is negligible, less than 0.5 cm/s.

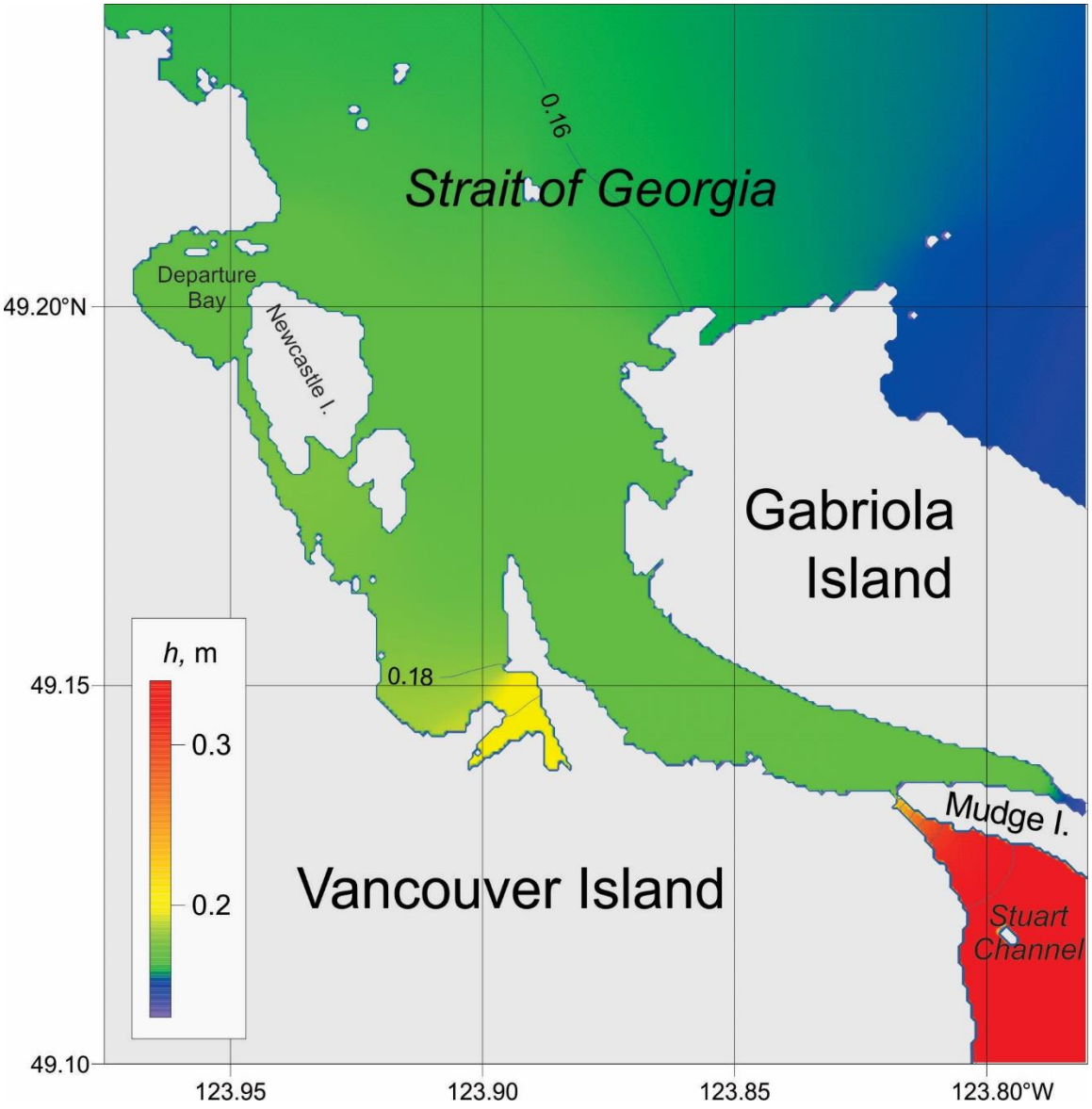

Figure 15. Distribution of maximum tsunami wave heights (*h*, metres) for Grid 3b (Nanaimo) of the nested-grid model for waves generated by simulation of a 1964-type Alaska tsunami.

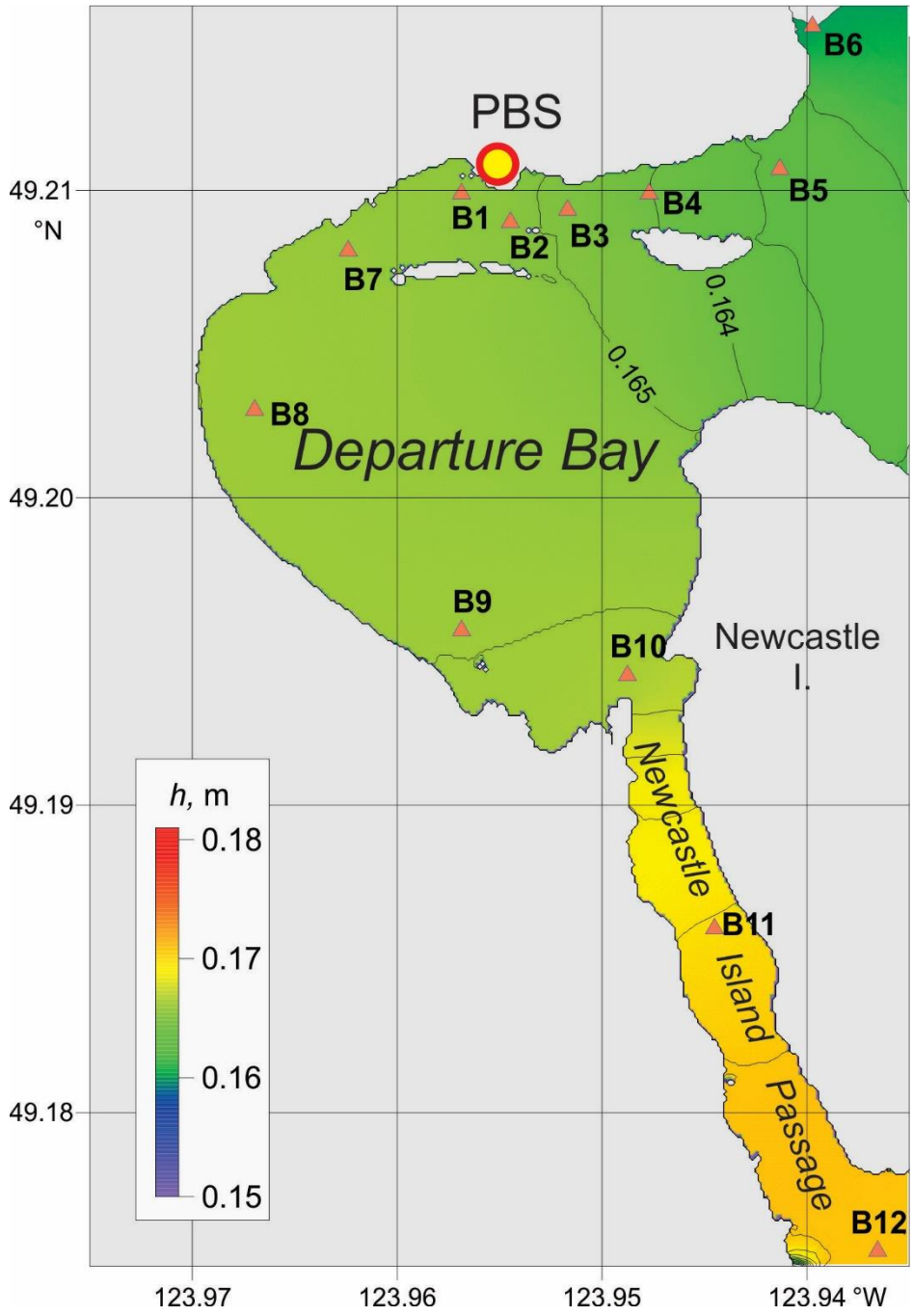

Figure 16. Distribution of maximum tsunami wave heights (h, metres) for Grid 4b (Departure Bay) of the nested-grid model for waves generated by simulation of a 1964-type Alaska tsunami.

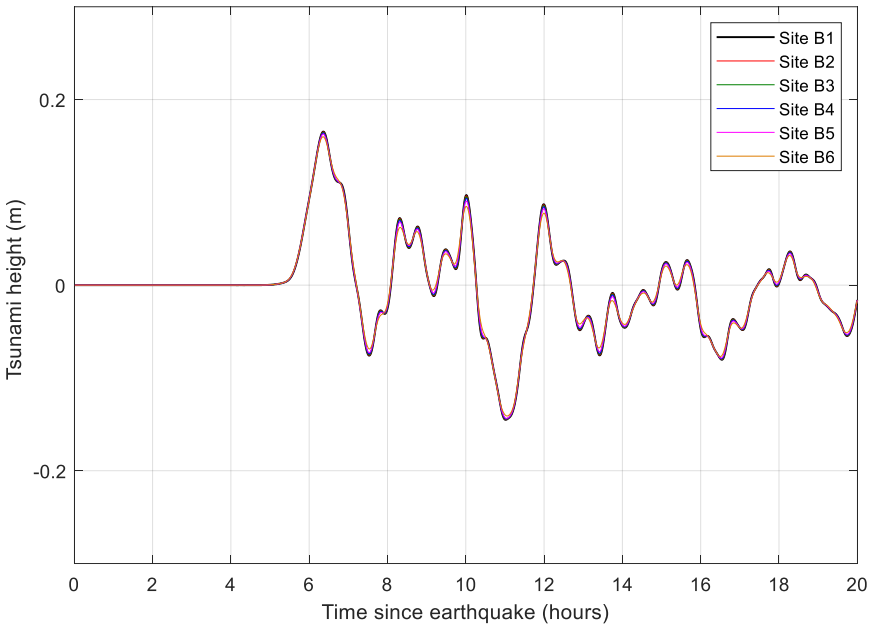

Figure 17. Simulated records of the tsunami waves for an Alaska 1964-type tsunami at Departure Bay sites B1, B2, B3, B4, B5 and B6 (See Figure 16 for the site locations).

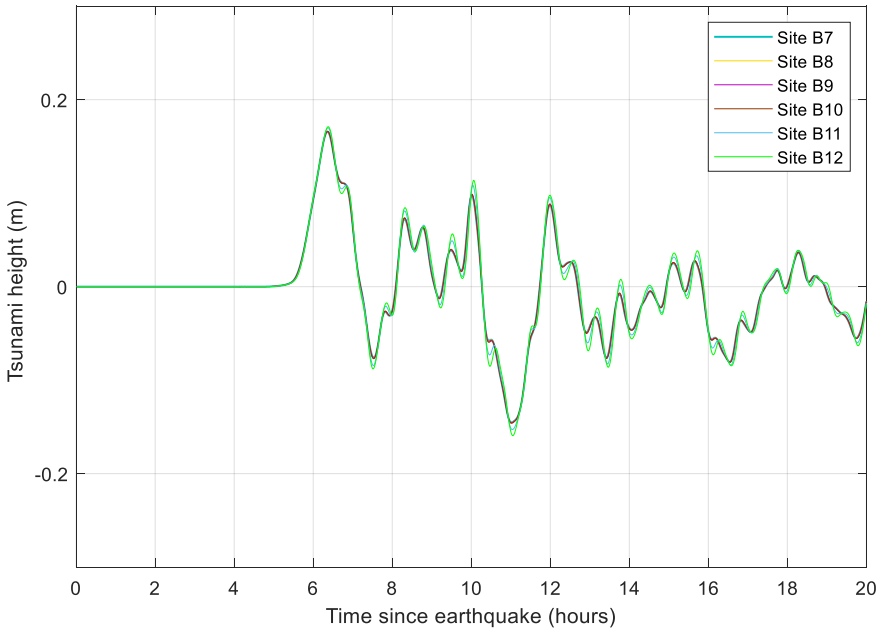

Figure 18. Simulated records of the tsunami waves for an Alaska 1964-type tsunami at Departure Bay sites B7, B8, B9, B10, B11 and B12 (See Figure 16 for the site locations). Note that the plots for all of the time series in this figure (and in Figure 17) fall nearly on top of one another so that they are not visible as separate curves in the figure.

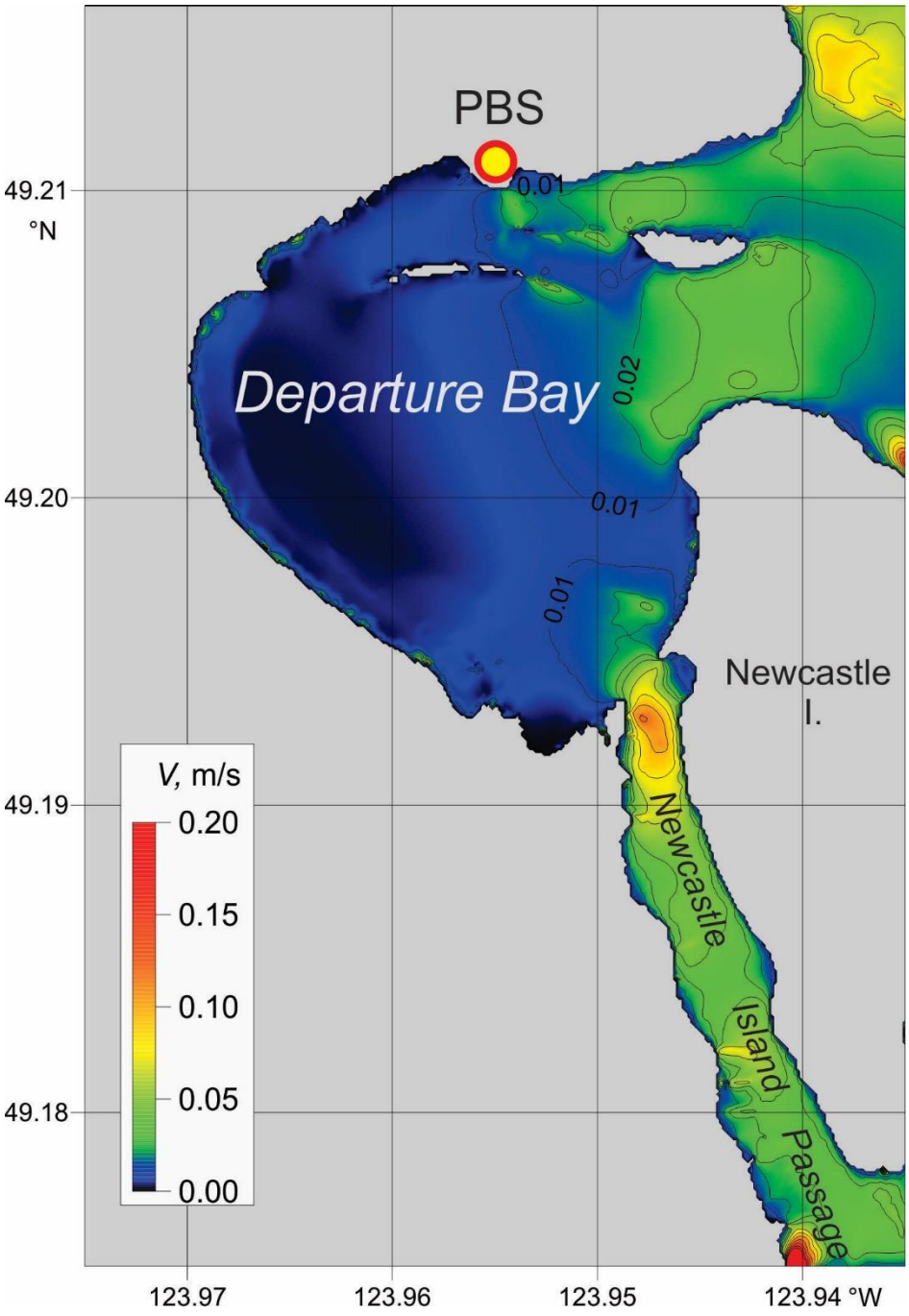

Figure 19. Distribution of maximum tsunami wave-generated currents (V, m/s) for Grid 4b (Departure Bay) for simulation of an Alaska1964-type tsunami.

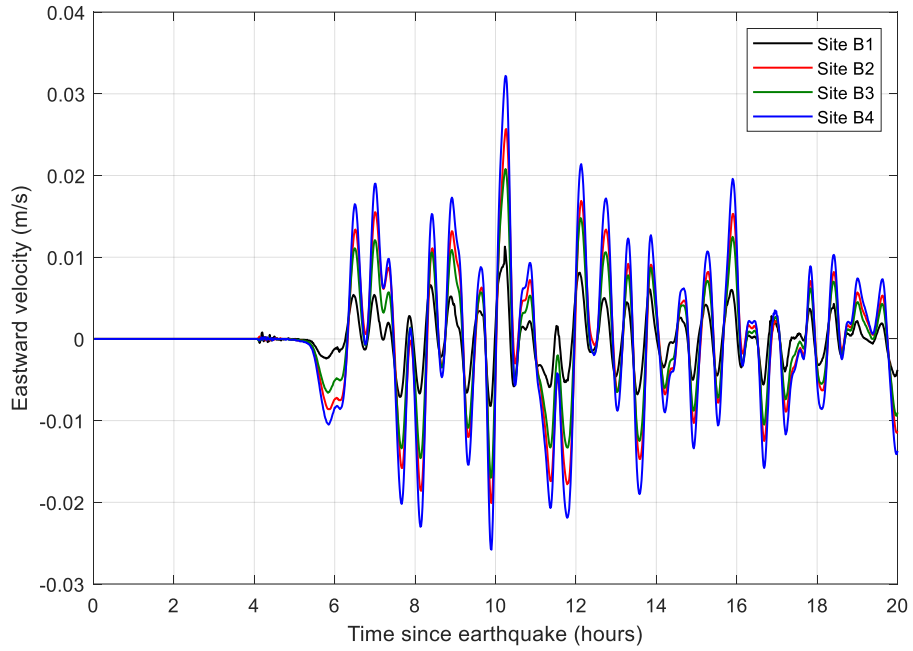

Figure 20. Simulated records of the eastward component of current velocity for an Alaska 1964-type tsunami at Departure Bay sites B1, B2, B3 and B4 (See Figure 16 for the site locations).

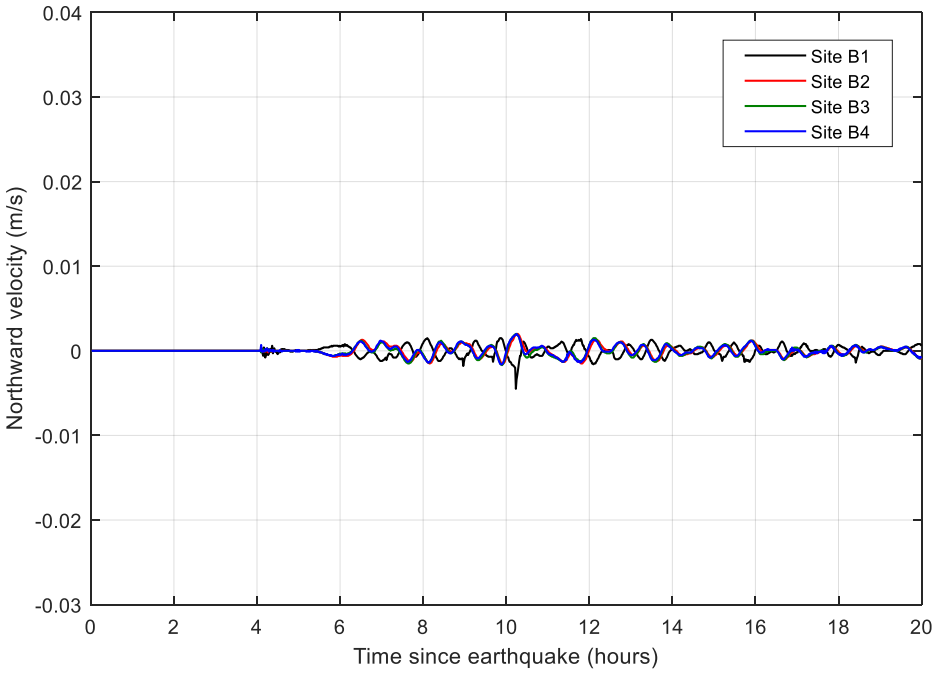

Figure 21. Simulated records of the northward component of current velocity for an Alaska 1964-type tsunami at Departure Bay sites B1, B2, B3 and B4 (See Figure 16 for the site locations).

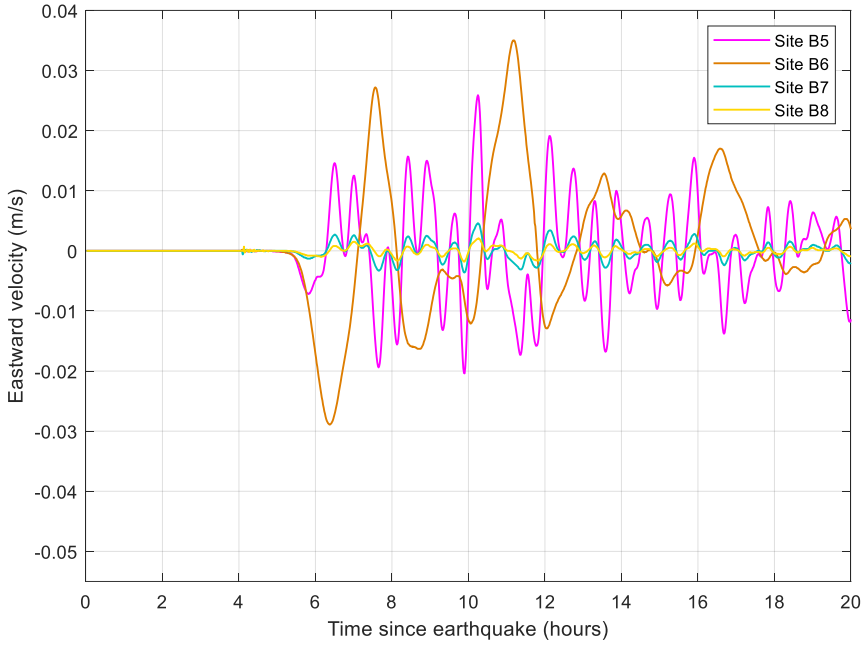

Figure 22. Simulated records of the eastward component of current velocity for an Alaska 1964-type tsunami at Departure Bay sites B5, B6, B7 and B8 (See Figure 16 for the site locations).

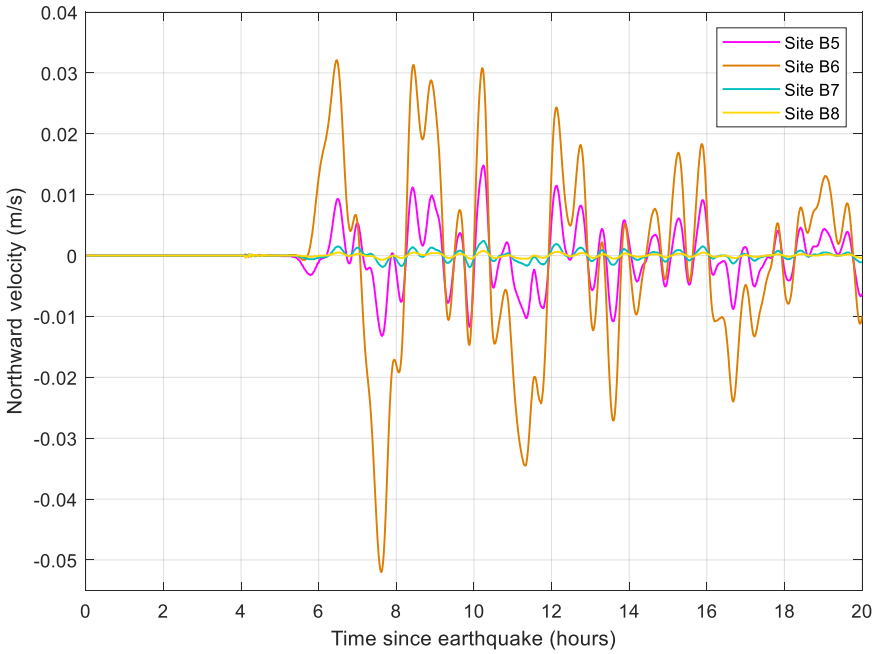

Figure 23. Simulated records of the northward component of current velocity for an Alaska 1964-type tsunami at Departure Bay sites B5, B6, B7 and B8 (See Figure 16 for the site locations).

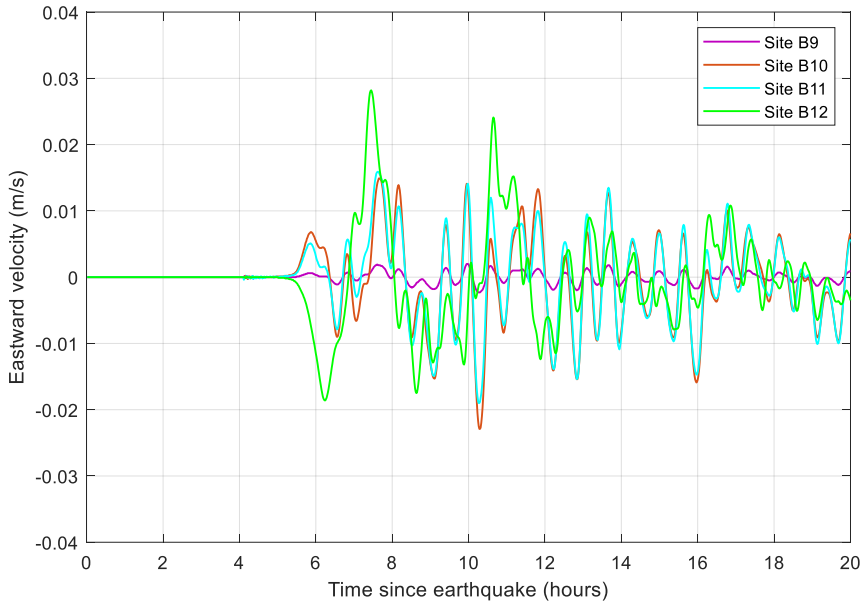

Figure 24. Simulated records of the eastward component of current velocity for an Alaska 1964-type tsunami at Departure Bay sites B9, B10, B11 and B12 (See Figure 16 for the site locations).

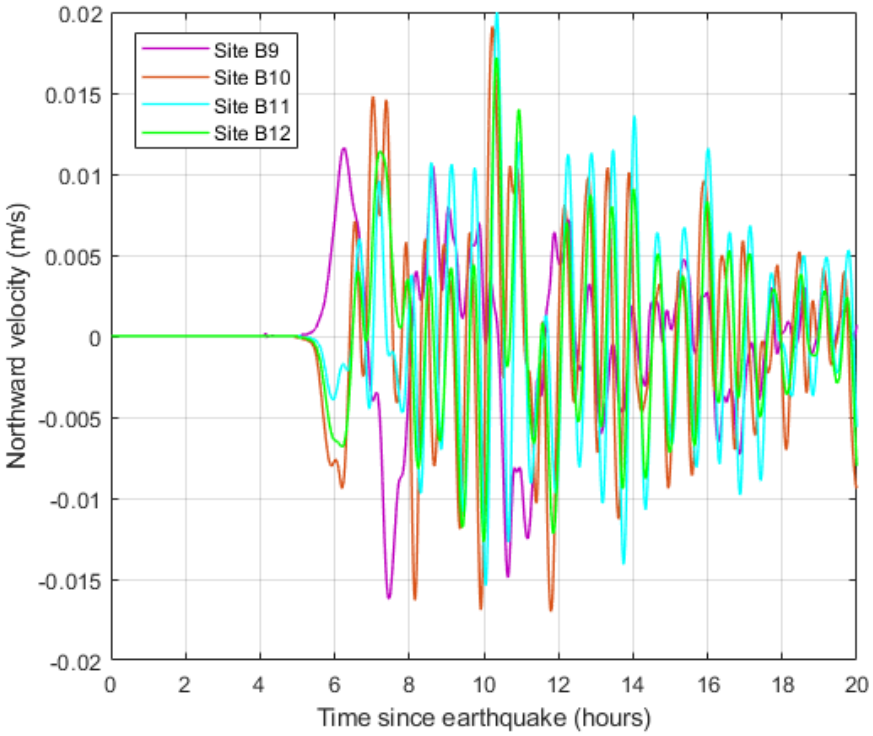

Figure 25. Simulated records of the northward component of current velocity for an Alaska 1964-type tsunami at Departure Bay sites B9, B10, B11 and B12 (Figure 16 shows the site locations).

6. CONCLUSIONS

A high-resolution, nested-grid tsunami model has been used to simulate tsunami waves and wave-induced currents that will be generated at the Institute of Ocean Sciences and co-located CCG station in Patricia Bay near Sidney and at the Pacific Biological Station in Departure Bay in Nanaimo during a major 1964-type Alaska tsunami. The model uses an advanced tsunami source distribution and high-resolution bathymetry and topography for the areas of interest. The primary results of the modelling are:

- The tsunami at the Patricia Bay Coast Guard Facility (Institute of Ocean Sciences) will reach 0.36 m above the tidal level at the time of the wave arrivals, with the third wave being the highest wave;
- The distribution of tsunami wave amplitudes at the Patricia Bay facility will be nearly spatially uniform;
- The tsunami will induce only weak currents near the Institute of Ocean Sciences and co-located CCG station, with maximum speeds below 0.2 m/s (0.4 knots);
- The tsunami at the Pacific Biological Station in Departure Bay (Nanaimo) will reach 0.16 m above the tidal level at the time of the wave arrivals, with the first wave being the highest wave;
- The tsunami wave amplitudes within Departure Bay will be almost spatially uniform;
- The tsunami will induce weak currents near the Pacific Biological Station, with maximum speeds below 0.05 m/s (0.1 knots);

Based on the numerical model results presented in this report, tsunami waves generated by an earthquake similar to the magnitude 9.2 Alaska earthquake of March 1964 are not a major threat to facilities at either the Institute of Ocean Sciences or the Pacific Biological Station under present-day sea level conditions. However, a future 1964-type tsunami event could posse a major hazard under global sea level rise conditions of up to 1 metre predicted by the year 2100. Additional numerical modeling under different global sea level rise scenarios may be required to determine the impact of sea level rise on the two facilities.

ACKNOWLEDGEMENTS

We thank Peter Wills and Tia Barlow of the Canadian Hydrographic Service (Institute of Ocean Sciences, Sidney, BC) for providing the bathymetric data and tide gauge records used in this study, and Elena Suleimani (University of Alaska at Fairbanks) for providing us the latest source model for the Alaska 1964-type earthquake and tsunami.

REFERENCES

Anderson, P.S., and Gow, G. A. (2004), *Tsunamis and Coastal Communities in British Columbia: An Assessment of the B.C. Tsunami Warning System and Related Risk Reduction Practices.*75xii pp. (Public Safety and Emergency Preparedness Canada, Ottawa)

Clague, J.J., Munro, A., and Murty, T.S. (2003), Tsunami hazard and risk in Canada, *Natural Hazards*, 28 (2-3), 433-461.

Dunbar, D., LeBlond, P., and Murty, T.S. (1991). Evaluation of tsunami amplitudes for the Pacific coast of Canada. *Progress in Oceanography*, 26, 115-177.

Fine, I.V., Cherniawsky, J.Y., Rabinovich, A.B., and Stephenson, F.E. (2008), Numerical modeling and observations of tsunami waves in Alberni Inlet and Barkley Sound, British Columbia, *Pure and Applied Geophysics*, 165 (11/12), 2019-2044.

Fine, I.V., Thomson, R.E., Lupton, L.M., and Mundschutz, S. (2018a). *Numerical Modelling of an Alaska 1964-type Tsunami at the Canadian Coast Guard Base in Seal Cove, British Columbia.* Canadian Technical Report of Hydrography and Ocean Sciences, 321: v + 33 p.

Fine, I.V., Thomson, R.E., Lupton, L.M., and Mundschutz, S. (2018b). *Numerical Modelling of an Alaska 1964-type Tsunami at the Canadian Coast Guard Base in Victoria, British Columbia.* Canadian Technical Report of Hydrography and Ocean Sciences, 323: v + 28 p.

Imamura, F., Yalciner, A.C. and Ozyurt, G. (2006). *Tsunami Modelling Manual (Tunami Model)*, 2006. http://www.tsunami.civil.tohoku.ac.jp/hokusai3/J/projects/manual-ver-3.1.pdf

Lander, J.F. (1996). *Tsunamis Affecting Alaska, 1737-1996*. Boulder, CO: U.S. Department of Commerce, 195 p.

Liu, P.L.-F., Woo, S.-B., and Cho, Y.-S. (1998). *Computer Programs for Tsunami Propagation and Inundation*. Technical report, Cornell University.

Myers, E.P., and Baptista, A.M. (2001). Analysis of factors influencing simulations of the 1993 Hokkaido Nansei-Oki and 1964 Alaska tsunamis. *Natural Hazards*, 23, 1-28; https://doi.org/10.1023/A:1008150210289

Rabinovich, A. B., Thomson, R. E., Krassovski, M. V., Stephenson, F. E., and D. C. Sinnott (2019). Five great tsunamis of the 20th Century as recorded on the coast of British Columbia, *Pure and Applied Geophysics*, 176, 2887–2924, doi:10.1007/s00024-019-02133-3.

Spaeth, M.G., and Berkman, S.C. (1967). *The Tsunami of March 28, 1964, as Recorded at Tide Stations.* Coast and Geod. Survey Techn. Bull. 33, US Department of Commerce, 86 p.

Suito, H., and Freymueller, J.T. (2009). A viscoelastic and afterslip post seismic model for the 1964 Alaska earthquake. *Journal of Geophysical Research*, 114, B11404, doi:10.1029/2008JB005954.

Suleimani, E.N., Nicolsky, D.J., and Koehler, R.D. (2013). *Tsunami Inundation Maps of Sitka, Alaska.* Report of Investigations 2013-3, State of Alaska, Department of Natural Resources, Division of Geological and Geophysical Surveys, Fairbanks, AK, 76 p., 1 sheet, scale 1:250,000. doi: 10.14509/26671.

Thomson, R.E., and Emery, W.J. (2024). *Data Analysis Methods in Physical Oceanography.* Fourth Edition. Elsevier, Amsterdam, 874 p.; https://doi.org/10.1016/B978-0-323-91723-0.00010-6

Wang, X. (2009). *User Manual for COMCOT Version 1.7*. http://ceeserver.cee.cornell.edu/pll-group/doc/COMCOT_User_Manual_v1_7.pdf.